This is a preprint, the final version is subject to change, of the American Mineralogist (MSA)
Cite as Authors (Year) Title. American Mineralogist, in press.
(DOI will not work until issue is live.) DOI: http://dx.doi.org/10.2138/am-2016-5722

Revision 1

Electron diffraction determination of 11.5 Å and HySo structures: candidate water carriers to the Upper Mantle

Mauro Gemmi[1], Marco Merlini[2], Lukáš Palatinus[3], Patrizia Fumagalli[2], Michael Hanfland[4]

[1]Center for Nanotechnology Innovation@NEST, Istituto Italiano di Tecnologia, Piazza S. Silvestro 12, 56127 Pisa, Italy.
[2]Dipartimento di Scienze della Terra "A. Desio", Università degli Studi di Milano, Via Botticelli 23, 20133 Milano, Italy.
[3] Institute of Physics of the AS CR, Na Slovance 2, Prague, Czech Republic.
[4] ESRF, The European Synchrotron Radiation Facility, 71, avenue des Martyrs, 38000 Grenoble, France

Corresponding author:

Mauro Gemmi
Center for Nanotechnology Innovation@NEST,
Istituto Italiano di Tecnologia,
Piazza S. Silvestro 12, 56127 Pisa, Italy.

E-mail: mauro.gemmi@iit.it

Abstract

The dehydration reactions of minerals in subduction zones strongly control geological processes, such as arc volcanism, earthquakes, serpentinization or geochemical transport of incompatible elements. In aluminium-bearing systems, chlorite is considered the most important hydrous phase at the top of the subducting plate, and significant amount of water is released after its decomposition. However, the dehydration mechanism is not fully understood, and additional hydrates are stabilized by the presence of Al beyond the stability field of chlorite. We applied here a cutting-edge analytical approach to characterize the experimental rocks synthesized at the high pressures and temperatures matching with deep subduction conditions in the upper mantle. Fast electron diffraction tomography and high resolution synchrotron X-ray diffraction allowed the identification and the successful structure solution of two new hydrous phases formed as dehydration product of chlorite. The 11.5 Å phase, $Mg_6Al(OH)_7(SiO_4)_2$, is a hydrous layer structure. It presents incomplete

tetrahedral sheets and face-sharing magnesium and aluminium octahedra. The structure has a higher Mg/Si ratio compared to chlorite, and a significantly higher density (ρ_0=2.93 g/cm^3) and bulk modulus (K_0=108.3(8) GPa), and it incorporates 13 wt% of water. The HySo phase, $Mg_3Al(OH)_3(Si_2O_7)$, is a dense layered sorosilicate, (ρ_0=3.13 g/cm^3 and K_0=120.6(6) GPa) with an average water content of 8.5 wt%. These phases indicate that water release process is highly complex, and may proceed with multistep dehydration, involving these layer structures whose features well match the high shear zones present at the slab-mantle wedge interface.

Keywords: Subduction, MASH system, electron diffraction tomography

Introduction

The knowledge of upper mantle mineralogy is necessary for the understanding of geophysical, petrological and geochemical processes occurring at inaccessible depths within the Earth (Fumagalli and Klemme 2015). Subsolidus phase relations at subduction zones are of particular interest as they involve hydrates as major characters of the deep water cycle of our planet.

In the past decades a significant effort was devoted to the recognition of hydrous phases in several compositional systems from the most simple (MgO-SiO_2-H_2O, - MSH, MgO, Al_2O_3, SiO_2- H_2O - MASH) to more complex chemical systems approaching natural bulk rocks of mainly mafic and ultramafic affinities expected to be representative of the input lithologies likely subducted.

The MSH system has been widely used as a reference for the hydrated mantle and the identification of a bunch of hydrous phases, called dense hydrous magnesium silicates - DHMS (Ohtani et al. 2000, Angel et al. 2001) stable beyond the serpentine and talc stability fields enrolled them as relevant water carriers at depth exceeding 100-150 km, e.g. phase A (Bose and Ganguly 1995) or 10 Å phase (Fumagalli et al. 2001). The MASH system has been widely used as a proxy not only of hydrated mantle rocks but also for hybrid rocks formed as a result of mass transfer at slab-mantle interface in subduction environments. Chlorite is the major relevant hydrate that has been extensively investigated in the MASH system as the major water carrier at mantle depth. Several additional Al-bearing hydrous phases of the MASH system and in more complex peridotite systems are stable beyond its stability field, e.g. the HAPY phase and the 11.5Å phase (Fumagalli et al. 2014), or the Al-bearing 10Å phase (Fumagalli and Poli 2005) and more recently it was claimed a new Al-bearing hydrous phase (called 23 Å) stable beyond the stability field of phase A (Cai et al. 2015). The stability field of hydrous phases is traditionally investigated by high-pressure experiments. While extensive technological innovation leads to significantly improved efficiency in generating high and ultra high pressure by means of solid media type multi anvil apparatus, the

obtained run products consist necessarily of nano-grained multi-phase materials, often of inaccessible size for conventional X-ray techniques. The complete characterization of high pressure charges (i.e. identification and structure determination of all phases present in the sample) is however desirable as a complete knowledge of all the potential candidate phases stable at variable pressures, temperatures and chemical compositions. This information may provide a valuable reference database, extremely useful for a full mineralogical and petrological understanding of the inner of our planet. In this process, the crystal structure determination of unknown phases stabilized at non-ambient condition experiments plays a primary role, and it is the first step to be pursued experimentally. This task can be particularly problematic if the sample is formed by single crystals of several phases having volume smaller than 10 μm^3, the most common case in high pressure experiments, when only X-ray powder diffraction (XRPD) analysis can be applied. XRPD is successfully used for the identification of known phases, but in the case of unknown structures the superposition of the scattering coming from different phases hampers a proper identification of the new ones. There is therefore a need to optimize alternative experimental methods and protocols for structural analysis.

The discovery of the HAPY phase, $Mg_{2.1}Al_{0.9}(OH)_2Al_{0.9}Si_{1.1}O_6$, (Gemmi et al. 2011) during a systematic investigation of high pressure experimental runs in the chlorite compositional system paved the route towards a method which combines EMPA and XRPD analyses with the unconventional electron diffraction tomography method (Kolb et al. 2007) which however was not yet optimized for routine analysis. The mineralogical information provided extremely new insights into water release mechanism at subduction zones and called for further investigations on chlorite (Fumagalli et al. 2014) and HAPY stability in a variable range of pressure and temperatures (table S1), providing materials containing new products. To investigate these new materials a completely new methodology for a fast electron diffraction screening was *ad hoc* developed.

The application of this methodology to the aforementioned materials resulted in the structural determination of two new hydrous phases, $Mg_6Al(OH)_7(SiO_4)_2$ and $Mg_3Al(OH)_3(Si_2O_7)$, both

observed as decomposition product of chlorite. The successful structure determination was achieved with a new protocol for electron diffraction analysis, combined with dynamical crystal structure refinement. This very recently developed technique (Palatinus et al. 2015a) allows a full structure refinement by electron diffraction, with accuracy comparable to XRD data. Both new phases have layered structures, with hitherto unknown topologies. $Mg_6Al(OH)_7(SiO_4)_2$ in particular can host 13 wt% of water and its possible occurrence in a wide pressure and temperature range reveals that the water recycling down to the transition zone through solid mineral carriers is a probable and very effective mechanism.

Materials and Methods

High pressure synthesis

High pressure synthesis was performed at the Dipartimento di Scienze della Terra in Milano, Italy, with a Walker type multianvil apparatus (Fumagalli and Poli 2005) using tungsten carbide cubes of 32 mm edge length and 17 mm truncation edge length (TEL); pressure cell was made of prefabricated MgO octahedra (containing 5 wt % of Cr_2O_3) with a 25 mm edge length (25M) and pyrophyllite gaskets. Pressure uncertainties, which largely depend on the accuracy of the calibrant reaction, were assumed to be 3%. Temperature was measured by S-type thermocouples and was considered accurate to 20 °C without taking into account any effect of pressure on the e.m.f. of the thermocouple.

In order to promote the synthesis at subsolidus conditions, a gel with the required $MgO:Al_2O_3:SiO_2$ molar proportions (Hamilton and Henderson 1968) has been prepared using tetraethylorthosilicate (TEOS) as silica source, pure Mg- and Al- nitric solutions. The gold capsule (outer diameter of 3.0 mm, length of 5 mm) was welded after being loaded with 10 mg of gel and 20 wt % of distilled water to achieve fluid saturated conditions, in the possible presence of chlorite minerals.

In the table 1 the synthesis conditions of the samples relevant for this study are summarized.

The experiments were performed in the system $Cr_2O_3–MgO–Al_2O_3–SiO_2–H_2O$. Starting from a Cr-clinochlore composition, $Mg_5(Al,Cr)_2Si_3O_{10}(OH)_8$, two different bulk compositions were prepared:

bulk A with Cr/(Cr + Al) = 0.075 and bulk B with Cr/(Cr + Al) = 0.25. The bulk JO lies on the join pyrope–phase A in the MASH system, with a composition of SiO_2 31.25 wt % Al_2O_3 12.5 wt % and MgO 56.25 wt % reflecting the preliminary composition of 11.5 A phase detected in run A8. All the details of synthesis protocols are reported in Fumagalli et al. (2014).

The run products were preliminary characterized by electron microprobe (JEOL JXA 8200) to check the mineral chemistry and the visible sample texture.

X-ray diffraction

The high resolution and in-situ high pressure X-ray powder diffraction were performed at the synchrotron ID09A beamline at ESRF, Grenoble, France (Merlini and Hanfland 2013). The standard beamline setup was used, with monochromatic beam with wavelength of 0.415 Å and flat panel Mar555 detector. High-resolution X-ray powder diffraction analysis was performed using 100x100x100 μm^3 fragments separated from the inner part of the experimental capsule, close to the portion analysed by microprobe and glued to a glass fiber or contained in a glass capillary. Data reduction and analysis was performed with Fit2D and GSAS software. The integrated powder patterns were fitted with the standard Rietveld procedure, using the crystallographic model of forsterite, pyrope clinoenstatite, guyanaite from literature, and the model for the 11.5 Å and HySo phase as result from the refinement against electron diffraction. The multiphase nature of all the samples, prevented any structural refinement, and only profile and lattice parameters were optimized. The Rietveld analysis approach provided also a quantitative estimation of the crystalline phases.

The high pressure experiments were performed using polycrystalline material in a membrane type DAC and methanol:ethanol mixture as pressure transmitting media. 17 pressure points were collected in the range 0-6 GPa. The extracted lattice parameters and volume were used for EoS fitting, with a 2^{nd} order Birch-Murnaghan equation of state with K'=4 (supplementary information).

Electron diffraction

Electron diffraction has been carried out at the Center for Nanotechnology Innovation@NEST on a Zeiss Libra120 operating at 120 kV equipped with an in-column omega filter for energy filtered imaging and a Nanomegas Digistar P1000 device for precession electron diffraction. Samples for electron diffraction were prepared by mild grinding of few milligrams of material recovered from the high pressure capsule on an agate mortar. The powder was then suspended in 2-propanol and a drop of the suspension was deposited on a carbon coated copper grid.

All the electron diffraction data have been collected in electron diffraction tomography mode. In this experimental modality the transmission electron microscope works as a single crystal electron diffractometer collecting a sequence of electron diffraction patterns while the crystal is tilted around the goniometer axis.

In the fast electron diffraction tomography (fEDT) mode, used for phase screening, the patterns are collected during the crystal rotation by recording an automatic sequence of frames with the CCD (Gemmi et al. 2015).

In the precession assisted EDT mode (PEDT), used for structure solution, the patterns are collected in precession mode (Vincent and Midgley 1994; Mugnaioli et al. 2009) manually by rotating the crystal in step of 1° and after each rotation, if necessary, the crystal is recentered under the electron beam. fEDT is fast but can cover only a limited angular range, usually around 40°, for stability limitation of the sample holder; PEDT is slower but the wider reciprocal space coverage and the quasi-kinematical character of the recorded intensities make PEDT intensities suitable for structure solution (Kolb et al. 2011).

PEDT data sets have been successfully used in the field of mineralogy and petrology for solving the crystal structure of several new minerals, such as charoite, vaterite, sarrabusite, widenmannite, cyanotrichite (Rozhdestvenskaya et al. 2010, Mugnaioli et al. 2012; Gemmi et al. 2012; Plášil et al. 2014, Ventruti et al. 2015), a high pressure polymorph of magnetite (Koch-Müller et al. 2014) and the HAPY phase – another high pressure phase of the MASH system (Gemmi et al. 2011). Details

of the all the fEDT and PED data collections can be found in the supplementary (table S1) and in table 2.

The data analysis of the fEDT and PEDT data collections have been performed with the software PETS (Palatinus 2011), while VESTA (Momma and Izumi 2011) has been used for the three dimensional visualization of the reciprocal space.

Dynamical refinement

Electrons strongly interact with matter and dynamical scattering occurs already in the smallest nanoparticles. For an accurate refinement of crystal structure against electron diffraction data kinematical diffraction theory is not sufficiently accurate and dynamical diffraction theory must be used. A method for the structure refinement against PEDT data has been developed and implemented in the computer program Jana2006 (Palatinus et al. 2013, Palatinus et al. 2015a, Palatinus et al. 2015b, Petříček et al. 2014). Application of this method does not require a separate diffraction experiment and standard PEDT data may be used. The key difference is that for each frame in the data collection the diffracted intensities are calculated separately using the dynamical diffraction theory. For this calculation, exact orientation of the frame with respect to the incoming beam must be known as well as the thickness of the crystal. Determination of these parameters is thus a part of the refinement process.

Another specialty of the dynamical refinement is the necessity to decide, which diffracted beams are considered close enough to the Bragg condition to be taken into account in a particular frame. A number of parameters were designed for this purpose (Palatinus et al. 2015a).:

- g_{max}: longest reciprocal lattice vector considered in the computation
- S_g^{max}(matrix): maximum excitation error for a reflection included in the computation of the calculated diffraction intensities
- S_g^{max} (refine): maximum excitation error for a reflection whose experimental intensity is considered in the least square procedure.

- R_{Sg}^{max}: it is specific to precessed data. It is the maximum ratio, accepted for a reflection to be considered in the refinement procedure, between the excitation error and the amplitude of the precession motion at the angle of the considered reflection. Its value, when smaller than 1, excludes from the refinement those reflections that are not properly sampled by the precession of the Ewald sphere.

Their influence on the structure refinement was thoroughly analyzed and their optimal values found on test structures using the criteria of both lower figure of merits and closer distance with the reference structures (Palatinus et al. 2015b). We used the recommended parameters in the refinement of the sorosilicate structure and their values can be found in table 2.

The dynamical refinement leads to a more accurate and more reliable structure model. Moreover, it allows the refinement of partial site occupancies and detection of partially occupied positions in the difference Fourier map. In the sorosilicate structure this refinement allowed the detection of partially occupied tetrahedral sites and thus a construction of a chemically and crystallographically coherent structure model. The improvement in the quality of the refinement over the kinematical refinement is demonstrated also in the improvement of all key figures of merit (see table 2).

Results

A procedure for phase screening of a synthetic microcrystalline rock

The identification of all the phases present in a polycrystalline run charge passes through a complete chemical and crystallographic characterization of the sample. In the case of a multi-phase sample with individual crystals of small size (i.e. <10 μm^3 in volume), there is the need to probe the sample with the highest available spatial resolution. The standard chemical characterization of the bulk sample (directly on the experimental charges) is usually performed with energy or wavelength dispersive spectrometry (EDS or WDS) in an electron microprobe (EMPA) or in a scanning transmission electron microscope (SEM). The crystallographic investigation is carried out through laboratory or synchrotron radiation powder x-ray diffraction (PXRD) on a grained fraction of the

recovered sample. A chemical analysis that does not match with the chemical composition of phases expected in the sample or/and the appearance of unknown diffraction peaks whose indexing is problematic are both possible signals of unknown crystal phases, but are not conclusive. A non-matching chemical composition can be due to mixed chemical analysis caused by the lack of spatial resolution in the electron probe available; unindexed diffraction peaks cannot be interpreted without a unit cell determination that in case of multiphase samples is strongly hampered by peak overlapping.

To solve the problem a single crystal diffraction technique able to collect diffraction patterns from single grains of small size (<1μm) is required and electron diffraction is a perfect candidate: it can be performed on crystals as small as a few tens of nanometers and it can be supported during the investigation by EDS spectroscopy. However, its use for phase screening of a powder sample requires establishing a fast procedure for the unit cell determination, which allows the investigation of several crystals in a single experimental session. Very recently a fast version of the so called electron diffraction tomography method (fEDT) has been proposed, in which a sequence of electron diffraction patterns covering an angular range of reciprocal space wide enough for the unit cell determination is collected for every crystal in less than 2 minutes (Gemmi et al. 2015). Once a phase having an unknown unit cell has been identified, the searching procedure can stop and its crystal structure can be further investigated using the standard precession-assisted electron diffraction tomography, PEDT (Mugnaioli et al. 2009), in which the sequence of electron diffraction patterns collected on the crystal is extended to the maximum angular range available (e.g. 90° to 120°). Due to the peculiar diffraction geometry of PEDT (random crystallographic orientation, beam precession), the PEDT intensities are quasi-kinematical and can be used for *ab initio* structure solution using methods based on kinematical scattering, like direct methods or charge flipping.

We can therefore define a procedure based on three main phases for the full determination of unknown crystal phases.

- A prescreening phase, via chemical analysis on an electron probe (SEM or EMPA) and PXRD, which identifies candidate samples hosting new phases through unusual chemical compositions and/or unindexed diffraction peaks in PXRD.
- An identification phase, in which fEDT identifies all the crystalline phases present in the candidate samples through the determination of their unit cells.
- A solution phase, in which the structure of crystal grains identified by their unusual unit cell as new phase candidates, is determined through PEDT analysis.

We report here the application of this procedure to the identification and structure determination of two new high-pressure phases in the MASH system.

New phases in chlorite system at deep subduction conditions

During a series of experiments designed for studying the influence of Cr in the high-pressure stability of chlorite (Fumagalli et al. 2014) we detected an indication of unknown phases through WDS/EDS EMPA analyses. Run conditions, together with starting bulk compositions and phase assemblages of experiments investigated in the present study are reported in Table 1. It is worth noting that a 4-phases assemblage and a 3-phases assemblages are in agreement with the Gibbs' phase rule for a 5 components system (Cr-MASH) and a 4 components system (MASH) respectively. Further experimental details can be found in the supplementary material. Several points analyses gave a composition highly rich in magnesium with a Mg:Al:Si atomic ratio close to 6:1:2 and a water content of 14-15 wt%. PXRD analysis supported the possible discovery of a new phase. The anomalous chemical composition was always associated with the presence of a diffraction peak corresponding to an interplanar distance of 11.5 Å, from which the name of 11.5Å phase for the candidate new phase. The presence of the 11.5 Å peak was detected in two different experiments at 6.5 GPa and 700 °C (table 1) and it was always associated with other phases, therefore PXRD was not effective for its structure determination. The fEDT screening on these samples allowed immediately to identify all the phases detected by PXRD (pyrope, forsterite, guyanaite) plus magnesite (see table S1), which is a product of the carbonatation of brucite due to a

long exposure of the sample to air. The TEM sample was observed after 2 years from its deposition. The fEDT screening is very effective and can be carried out on small crystals (<500nm), not necessarily isolated as demonstrated by the two aggregates displayed in fig. 1.

In addition to known phases fEDT detected also a disordered phase which exhibits a 11.5 Å periodicity and has the characteristic features of a layered silicate: a strong streaking along the direction corresponding to the longest periodicity (11.5 Å); the plane normal to this direction that has the geometry of a phyllosilicate building module (a rectangular centered lattice with parameters a=8.9 Å and b=5.1 Å, fig. 2a and 2b); a streaking behavior in the sections of the reciprocal space normal to those directions that in case of a mica structure would correspond to [010] and [110] respectively (fig. 2c and 2d), that is characteristic of a stacking disorder in a mica polytype (Kogure and Nespolo 1999, Fregola et al. 2009).

In order to find an ordered polytype we started a survey of systematic observations on the sample JO1 in which the concentration of the 11.5 Å phase was the highest. After several TEM sessions we found a crystal that in a bright field image was showing an area of few hundred nm apparently free of defects (fig. S1). The three dimensional reconstruction of the reciprocal space from data collected in this area revealed a scattering almost free from streaking with sharp spots and allowed a reliable unit cell determination (fig. 3). The extracted monoclinic unit cell can index most of the diffraction lines in high resolution PXRD.

The fEDT screening for an ordered 11.5 Å phase in JO1 sample revealed also the presence of a second phase having a chemical composition with a Mg:Al:Si atomic ratio close to 3:1:2 and whose unit cell was surprisingly not matching any known mineral in the MASH system. fEDT applied to few grains of this phase revealed that it is monoclinic and its lattice was able to index the remaining diffraction lines in PXRD pattern of the JO1 sample. This unit cell can also successfully explain some unindexed diffraction peaks observed in the other two syntheses with a Cr-enriched chlorite bulk composition at 6.0 GP, 650°C and 6.5 GPa, 700 °C (table 1). The structure determination of the two newly identified phases is described in the following two sections

298 **11.5Å - $Mg_6Al(OH)_7(SiO_4)_2$ crystal structure: a new hydrous layer silicate**

299 The ordered 11.5 Å phase is C-centered monoclinic with a=9.012(1) Å b=5.201(1) Å c=23.202(5)
300 Å β=97.8°(1) (as refined by PXRD), and the reflections are compatible with a *C1c1* extinction
301 symbol. Depending on the presence of the inversion center the possible space groups are *Cc* or
302 *C2/c*. We solved the structure with direct methods, with SIR2011 (Burla et al. 2012) and charge
303 flipping, with Superflip (Palatinus and Chapuis 2007) and in both cases we obtained a reliable
304 model in *C2/c*. The final model refined with Jana2006 (kinematical refinement) is displayed in fig.
305 3. The data collection parameters and the figure of merits of the refinements are reported in table 2.
306 The atomic positions after kinematical refinement are reported in the supplementary (table S2).
307 The hypothesis of the structure as a stacking sequence of tetrahedral and octahedral layers is
308 correct, but it does not correspond to any known silicate. The basic stacking sequence consists of T-
309 O-T-like groups connected by a double di-octahedral layer of face sharing octahedra (O-O). In the
310 T-O-T-like module the octahedral layer is tri-octahedral (i.e. talc-like), while the T layer is
311 incomplete and formed by isolated tetrahedra, since only one out of three tetrahedral sites is
312 occupied. One unit cell consists of a sequence of two different T-O-T/O-O blocks, which differ by
313 the way in which the second T-layer is stacked onto the O-layer. Cation ordering arises in the O-
314 layers with one octahedron of the T-O-T group having an average cation oxygen distance smaller
315 than 2 Å compatible with a full Al occupancy, while all the others octahedral sites have a larger
316 cation-oxygen distance compatible with a Mg occupancy (table S2).
317 Making the assumption of tetrahedral sites being fully occupied by Si, we obtain for the phase the
318 chemical formula $Mg_6Al(OH)_7(SiO_4)_2$, in which the number of OH is determined from the
319 electroneutrality. This requires that all the oxygen atoms except for those belonging to SiO_4 groups
320 are hydroxyls: the oxygen layer shared by the face sharing octahedra is an OH layer and 2/3 of the
321 oxygen in the O-layer of the T-O-T group are hydroxyls. On the basis of the derived chemical
322 formula the water content should be 13.2 wt%, very close to the measured WDS value of 14-15

wt% (table S5). The density of $Mg_6Al(OH)_7(SiO_4)_2$ at ambient conditions is noticeably high, 2.93 g/cm^3.

The mechanism that controls the stacking disorder can be easily understood by observing that the low tetrahedral density in the T-layer offers a variability in which the tetrahedra of the second T-layer connect to the O-layers in a T-O-T block. Depending on which of the three possible tetrahedral sites is occupied, the center of the tetrahedra in each second T-layer can be shifted along [1,1,0], [1-1,0] or [0,1,0] with respect to the tetrahedra of the first layer. In the observed ordered form of 11.5 Å phase we have an alternating shift along [1,1,0] and [1,-1,0] in two successive T-O-T blocks, which is responsible for the doubling of the unit cell along *c* (fig. S2). In the nomenclature of layered polytypes the ordered 11.5 Å phase is a $2M_2$ polytype. In the case of the most common disordered phase the stacking sequence in the T-O-T layers is random with different shifts in every second T-layer, a mechanism well known in disordered layered silicates. A high resolution image taken in orientation [110], in which the different shifts of the T layers can be distinguished, confirms this interpretation. A comparison with a simulation based on the ordered model shows that the shift of the T-layer in two successive T-O-T modules varies in an irregular way (fig. 5). A further confirmation of the correctness of the model comes from Rietveld refinement which allows a perfect fit of high-resolution X-ray powder diffraction pattern of JO1 sample (fig. 6).

HySo - $Mg_3Al(OH)_3(Si_2O_7)$ crystal structure: a new hydrous sorosilicate

The unit cell determination from fEDT of the second phase, results in a monoclinic C-centered unit cell with parameters a=9.150(1) Å b=14.74(1) Å c=5.071(5) Å β=98.30°(5) (as refined by PXRD). This phase has sharp diffraction peaks, and PEDT analysis does not show any additional extinction condition to the centering, giving an extinction symbol of *C1-1* compatible with *C2, Cm* and *C2/m* space groups (fig. 7).

The crystal structure was solved with direct methods, with SIR2011 (Burla et al. 2012) and a chemically sound solution was achieved only in the centrosymmetric space group *C2/m* (see table S3). The ab-initio structural model obtained with PEDT data indicates that the new phase is a

sorosilicate (fig. 8a, 8b). The main building blocks are octahedral layers hosting Mg and Al parallel to the *b*-*c* plane, connected along *a* by stripes of isolated Si_2O_7 groups running parallel to *c* direction. In each stripe the tetrahedral apical oxygens point all in the same direction (positive or negative *a* direction), which is reversed in nearby stripes. In the octahedral layer all the octahedral sites are occupied except those two that sit below the Si_2O_7 groups which connect two consecutive layers. If we consider that the tetrahedral sites are fully occupied by Si, and if we further take into account the measured Mg:Al ratio of 1:3, the multiplicity of the octahedral sites and the electroneutrality constraint, we obtain for the new phase the chemical formula $Mg_3Al(OH)_3(Si_2O_7)$, which implies that all oxygen sites but those coordinated to a tetrahedral site are occupied by OH groups. The sorosilicate is therefore hydrous from which the name HySo. The derived structural model can reproduce the intensity observed in XRPD patterns (fig. 6) and allows, through a Rietveld refinement and together with the 11.5 Å phase model, a quantitative estimation of the crystalline phases present in the samples in which it arises (fig. S5-S7, table S6).

Although chemically coherent, this represents an average model which does not fit perfectly the PEDT data. In fact the M5 octahedral site, which shows a quite distorted coordination with two long cation oxygen distances of 2.4 Å, is not retrieved in all structure solutions with different PEDT data sets (we have collected 7 PEDT data sets on different crystals, see supplementary, table S3), and when it is detected, its electron density is very low, indicating a possible partially occupied site. By applying a refinement procedure which takes into account dynamical scattering (see materials and methods), the partial occupancy of the M5 sites is confirmed and a difference Fourier map shows previously undetected tetrahedral sites (fig. 8c). These tetrahedral sites (T-sites), T2, T3, are too close to the M5 and M4 octahedra respectively, therefore they can be occupied only if the corresponding octahedron is empty. From chemical considerations on the electroneutrality of the chemical formula and from the multiplicity of the different sites, the chemical formula of the defective compound becomes $(Mg_{3+0.5xT2+xT3}Al)(OH)_{3-xT2-2xT3}O_{xT2+2xT3}(Si_2O_7)$, where x_{T2} x_{T3} are the occupancies of T2 and T3 respectively (see supplementary for a detailed derivation). The formation

of a defective structure involves a release of water and an incorporation of an equivalent number of moles of MgO, therefore the total number of oxygens in the cell is conserved and only Mg and H are exchanged.

The final model was refined with the constraints $x_{T2}+x_{M5}=1$ and $x_{T3}+x_{M4}=1$, to avoid simultaneous occupancy of adjacent T and O sites and yielded $x_{T2}=0.203(7)$ and $x_{T3}=0.209(6)$ (see table 2 for the parameters of the refinement, table S4 for the refined atomic positions and the interatomic distances).

The chemical formula of the vacancy model refined with PEDT data can then be approximated as $Mg_{3.30}Al((OH)_{2.40}O_{0.60})(Si_2O_7)$. The vacancy model implies that the new phase is not a sorosilicate *"sensu stricto"*, but the Si_2O_7 can be connected by other two or three tetrahedra forming larger clusters in the tetrahedral layers (see fig. 8d).

The ideal stoichiometry indicates that this phase may incorporate up to 8.5 wt % of water. The density of $Mg_3Al\ (OH)_3(Si_2O_7)$ at ambient condition is 3.13 g/cm^3.

Implications

The 11.5Å phase $Mg_6Al(OH)_7(SiO_4)_2$ and HySo $Mg_3Al(OH)_3(Si_2O_7)$ represent two new structural types among the known hydrous silicates and significantly increase the number of hydrous phases in the MASH system that play an active role in the water exchange at subduction conditions (table 3).

The 11.5Å-phase is a layer silicate, with structural features typical of high pressure phases. It is built from modular blocks constituted by double octahedral and T-O-T layers. All the connections in the structure are by corner-, edge- and face-sharing of the constituting Si, Al and Mg tetrahedra and octahedra. In particular, the face sharing MgO_6 octahedra (fig. 4) are responsible for the high density of the phase, comparable to hydrous phase A and E (2.96 and 2.88 g/cm3 respectively). Contrary to the common phyllosilicates in mafic and ultramafic rocks (e.g chlorite, talc or serpentine), the 11.5Å phase structure does not present layer units connected by hydrogen bond. This structural feature can explain its elastic behavior with a high bulk modulus $K_0=108.3(8)$ GPa

(as determined by in-situ synchrotron X-ray powder diffraction, see supplementary). This value is visibly higher than other Mg-Al hydrous silicates, e.g. chlinoclore, K_0=75 GPa (Welch and Marshall 2001); 10Å-phase, K_0=39 GPa (Comodi et al. 2006); talc, K_0=56 GPa (Gatta et al. 2013), and also slightly higher than phase A (K_0=105 GPa (Kudoh et al. 2002), K_T=97, K_T'=6 (Crichton and Ross 2002)), which exhibits similar density and water content. The axial compressibility is quite isotropic, with the *c*-axis only slightly more compressible than *a*-*b* (fig. S11). A situation different from the known layer silicates, where a strong elastic anisotropy related to the shrinking of O-H..O bonds is normally observed. These features were noticed also for the elastic behavior of phase A (Sanchez-Valle et al. 2008), which seems to be the MSH analogous of 11.5Å phase.

The 11.5Å phase must be closely related with a recently discovered hexagonal hydrous Mg-Al silicate phase synthesized at 10 GPa and 1000 °C (Cai et al. 2015). Its hexagonal unit cell, if described with the crystallographic reduced C-centred monoclinic unit cell, is similar to the unit cell of the 11.5Å phase, as well as its determined crystal chemistry, $Mg_{11}Al_2Si_4O_{16}(OH)_{12}$. We can suppose that either a quenchable hexagonal high-pressure polymorph of 11.5Å phase exists or, alternatively, that the X-ray powder diffraction pattern could not resolve the monoclinic symmetry.

The crystal chemistry of the 11.5Å phase is compatible with the bulk chemical composition of the "hybrid rocks" (Spandler et al. 2008) existing at the slab interface in subduction environments (Fumagalli and Poli 2005). The petrological significance of the 11.5Å-structure is far reaching. In the simplified MgO-SiO_2-H_2O system (MSH), we observe, at low pressures, hydrous phyllosilicate phases such as serpentine and talc. Their role as water carriers or water hosting minerals in the upper portion of the upper mantle is well recognized. The breakdown of these structures proceed, along a subduction geotherm, with the stabilization of the phase A, which exhibits completely new crystallographic features, in particular the presence of isolated SiO_4 tetrahedra and OH groups with hydrogen atoms located in structural interstices. Consequently, the density of phase A is significantly higher as well as its water storage capability. In the MgO-Al_2O_3-SiO_2-H_2O (MASH)

system, the determination of 11.5Å-phase indicates a similar structural scenario. The low pressure phyllosilicate phases, chlorite in particular, on increasing pressure and temperature, destabilize with the formation of new types of phases, no longer based on infinite tetrahedral layers, and hydrogen bond as connection mechanism between the structural modules. The Si-O-Si interconnections are therefore reduced and the density is significantly increased. This is the case of 11.5Å and HySo phase reported here, as well the HAPY structure (Gemmi et al. 2011).

The above considerations apply also for the HySo phase $Mg_3Al(OH)_3(Si_2O_7)$, which has a high bulk modulus K_0=120.6(6) GPa (see supplementary and fig. S11). It is noticeable, for HySo, the defect mechanism based on octahedral vacancies revealed by electron-diffraction single-crystal structure refinements. Exploiting this mechanism HySo can host a variable amount of water acting as a water reservoir. In principle HySo can adapt its water content by exchanging Mg with the environment in a window of a few wt% of water until the vacancies in the octahedral layer make the structure to collapse.

The occurrence of 11.5Å and HySo phases as breakdown product of a clinochlore composition suggestscon that, for Al-enriched hybrid rocks in subduction environments, they can effectively act as water carrier beyond the stability field of chlorite in the upper Earth's Mantle.

An obvious question arises: what will be the role of these phases in more complex systems? Although it is difficult to speculate we can confidently affirm that these crystal structures can host iron in both its oxidation states, Fe^{2+} substituting Mg in the octahedral sites and Fe^{+3} substituting Al in tetrahedral sites in proportions depending on oxygen fugacity, and small quantities of Ca can be hosted by HySo in the M5 site. In this respect we can envisage that the presence of garnet would play an important role on the stability of both phases if Fe is added to the system.

The results here obtained are remarkable also from a methodological point of view. The proposed combination of fEDT plus PEDT for the phase screening and crystal structure determination of nanocrystal, if applied systematically to high pressure experimental charges will allow the

452 discovery of several new phases, and the correct interpretation of experiments, where x-ray
453 diffraction and EMPA analysis give contradictory results.

454
455 **References**
456

457 Angel, R.J., Frost, D.J., Ross, N.-L., and Hemley, R. (2001) Stabilities and equations of state of
458 dense hydrous magnesium silicates. Physics of the Earth and Planetary Interiors, 127, 181–196.

459 Bose, K., and Ganguly, J. (1995) Experimental and theoretical studies of the stabilities of talc,
460 antigorite and phase A at high pressures with applications to subduction processes. Earth and
461 Planetary Science Letters, 136, 109-121.

462 Brown, B.E., and Bailey, S.W. (1963) Chlorite polytypism: II. Crystal structure of a one-layer Cr-
463 chlorite. American Mineralogist, 48, 42-61.
464
465 Burla, M.C., Caliandro, R., Camalli, M., Carrozzini, B., Cascarano, G.L., Giacovazzo, C., Mallamo,
466 M., Mazzone, A., Polidori, G., and Spagna, R. (2012) SIR2011: a new package for crystal structure
467 determination and refinement. Journal of Applied Crystallography, 45, 357–361.

468 Cai, N., Inoue, T., Fujino, K., Ohfuji, H., and Yurimoto, H. (2015) A possible new Al-bearing
469 hydrous Mg silicate (23 Å phase) in the deep upper mantle. American Mineralogist, 100, 2330-
470 2335.
471
472 Comodi, P., Cera, F., Dubrovinsky, L., and Nazzareni, S. (2006) The high-pressure behaviour of the
473 10 Å phase: A spectroscopic and diffractometric study up to 42 GPa. Earth and Planetary Science
474 Letters, 246, 444–457.
475
476 Crichton, W.A., and Ross, N.L. (2002) Equation of state of dense hydrous magnesium silicate phase
477 A, Mg7Si2O8(OH)6. American Mineralogist, 87, 333-338.
478
479 Fregola, R.A., Capitani, G., Scandale, E., and Ottolini, L. (2009) Chemical control of 3T stacking
480 order in a Li-poor biotite mica. American Mineralogist, 94, 334-344.
481
482 Fumagalli, P., Sixtrude, L., Poli, S., and Snyder, D. (2001) The 10Å phase: A high-pressure
483 expandable sheet silicate stable during subduction of hydrated lithosphere. Earth Planetary Science
484 Letters, 186, 125-141.
485
486 Fumagalli, P., and Poli, S. (2005) Experimentally determined phase relations in hydrous peridotites
487 to 6.5 GPa and their consequences on the dynamics of subduction zones. Journal of Petrology, 46,
488 555-578.
489
490 Fumagalli, F., Poli, S., Fischer, J. K., Merlini, M. and Gemmi, M. (2014) The high-pressure
491 stability of chlorite and other hydrates in subduction melanges: experiments in the system Cr_2O_3-
492 MgO-Al_2O_3-SiO_2-H_2O. Contribution to Mineralogy and Petrology, 167, 979.
493
494 Fumagalli, P., and Klemme, S. (2015) Mineralogy of the Earth: Phase Transitions and Mineralogy
495 of the Upper Mantle. In G. Schubert, Ed., Treatise on Geophysics, 2nd Edition, p. 7-31. Elsevier,
496 Oxford, UK.

497 Gatta, G.D., Merlini, M., Valdrè, G., Liermann, H.P., Nénert, G., Rothkirch, A., Kahlenberg, V.,
498 and Pavese A. (2013) On the crystal structure and compressional behavior of talc: a mineral of

interest in petrology and material science. Physics and Chemistry of Minerals, 40, 145-156.

Gemmi, M., Fischer, J.K., Merlini, M., Poli, S., Fumagalli, P., Mugnaioli, E., and Kolb U. (2011) A new hydrous Al-bearing pyroxene as water carrier in subduction zones. Earth and Planetary Science Letters, 310, 422-428.

Gemmi, M., Campostrini, I., Demartin, F., Gorelik, T.E., and Gramaccioli, C.M.(2012) Structure of the new mineral sarrabusite, $Pb_5CuCl_4(SeO_3)_4$, solved by manual electron-diffraction tomography. Acta Crystallographica, B68, 15-23.

Gemmi, M., La Placa, M.G.I., Galanis, A., Rauch, E.F., and Nicolopoulos, S. (2015) Fast electron diffraction tomography. Journal of Applied Crystallography, 48, 718-727.

Gottschalk, M., Fockenberg, T., Grevel, K.D., Wunder, B., Wirth, R., Schreyer, W., and Maresch, W.V. (2000) Crystal structure of the high-pressure phase $Mg_4(MgAl)Al_4(Si_6O_{21}/(OH)_7)$: an analogue of sursassite. European Journal of Mineralogy, 12, 935-945.

Hamilton, D.L., and Henderson, C.M.B. (1968) The preparation of silicate composition by gelling method. Mineralogical Magazine, 36, 832–838.

Koch-Müller, M., Mugnaioli, E., Rhede, D., Speziale, S., Kolb, U., and Wirth, R. (2014) Synthesis of a quenchable high-pressure form of magnetite (h-Fe_3O_4) with composition $^{Fe1}(Fe^{2+}_{0.75}Mg_{0.26})^{Fe2}(Fe^{3+}_{0.70}Cr_{0.15}Al_{0.11}Si_{0.04})_2O_4$. American Mineralogist, 99, 2405-2415.

Kogure, T., and Nespolo, M. (1999) First occurrence of a stacking sequence including (±60°, 180°) rotations in Mg-rich annite. Clays and Clay Minerals, 47, 784-792.

Kolb, U., Gorelik, T.E., Kübel, C., Otten, M.T., and Hubert, D. (2007) Towards automated diffraction tomography: Part I—data acquisition. Ultramicroscopy, 107, 507–513.

Kolb, U., Mugnaioli, E., and Gorelik, T.E. (2011) Automated electron diffraction tomography – a new tool for nano crystal structure analysis. Crystal Research and Technology, 6, 542-554.

Kudoh, Y., Kuribayashi, T., Kagi, H., Sasaki, S., and Tanaka, M. (2002) High-pressure structural study of phase-A, $Mg_7Si_2O_8(OH)_6$ using synchrotron radiation. Journal of Physics: Condensed Matter, 14, 10491–10495.

Merlini, M., and Hanfland, M. (2013) Single crystal diffraction at megabar conditions by synchrotron radiation. High Pressure Research, 33, 511-522.

Momma, K., and Izumi, F. (2011) VESTA 3 for three-dimansional vizualisation of crystal, volumetric and morphology data. Journal of Applied Crystallography, 44, 1272–1276.

Mugnaioli, E., Gorelik, T.E., and Kolb, U. (2009) Ab initio structure solution from electron diffraction data obtained by a combination of automated electron diffraction tomography and precession technique. Ultramicroscopy, 109, 758–765.

Mugnaioli, E., Andrusenko, I., Schüler, T., Loges, N., Dinnebier, R.E., Panthöfer, M., Tremel, W., and Kolb, U. (2012) Ab initio structure determination of vaterite by automated electron diffraction. Angewande Chemie International Edition, 51, 7041-7045.

Ohtani, E., Mizobata, H., and Yurimoto, H. (2000) Stability of dense hydrous magnesium silicate hases in the systems Mg_2SiO_4-H_2O and $MgSiO_3$-H_2O at pressures up to 27 GPa. Physics and chemistry of minerals, 27, 533-544.

Palatinus, L., and Chapuis, G. (2007) Superflip - a computer program for the solution of crystal structures by charge flipping in arbitrary dimensions. Journal of Applied Crystallography, 40, 786-790.

Palatinus L (2011) PETS—software for processing of electron diffraction data. Institute of Physics,

Praha, Czech Republic.

Palatinus, L., Jacob, D., Cuvillier, P., Klementová, M., Sinkler, W., and Marks, L.D. (2013) Structure refinement from precession electron diffraction data. Acta Crystallographica, A69, 171–188.

Palatinus, L., Petříček, V., and Corrêa, C.A. (2015a) Structure refinement using precession electron diffraction tomography and dynamical diffraction: theory and implementation. Acta Crystallographica, A71, 235-244.

Palatinus, L., Corrêa, C.A., Steciuk, G., Jacob, D., Roussel, P., Boullay, P., Klementová, M., Gemmi, M., Kopecek, J., Domeneghetti, M.C., Cámara, F., and Petrícek, V. (2015b) Structure refinement using precession electron diffraction tomography and dynamical diffraction: tests on experimental data. Acta Crystallographica, B71, 740-751.

Petříček, V., Dušek, M., and Palatinus, L. (2014) Crystallographic computing system JANA2006: general features. Zeitschrift für Kristallographie, 229 ,345–352.

Plášil, J., Palatinus, L., Rohlíček, J., Houdková, L., Klementová, M., Goliáš, V., and Škácha, P. (2014) Crystal structure of lead uranyl carbonate mineral widenmannite: precession electron-diffraction and synchrotron powder-diffraction study. American Mineralogist, 99, 276-282.

Rozhdestvenskaya, I., Mugnaioli, E., Czank, M., Dempmeier, W., Kolb, U., Reinholdt, A., and Weirich, T. (2010) The structure of charoite, $(K,Sr,Ba,Mn)_{15–16}(Ca,Na)_{32}[(Si_{70}(O, OH)_{180})](OH,F)_{40}.nH_2O$, solved by conventional and automated electron diffraction. Mineralogical Magazine, 74,159–177.

Sanchez-Valle, C., Sinogeikin, S.V., Smyth, JR., and Bass, J.D. (2008) Sound velocities and elasticity of DHMS phase A to high pressure and implications for seismic velocities and anisotropy in subducted slabs. Physics of the Earth and Planetary interior, 170, 229-239.

Spandler, C., Hermann, J., Faure, K., Mavrogenes, J.A., and Arculus, R.J. (2008) The importance of talc and chlorite ‘‘hybrid’’ rocks for volatile recycling through subduction zones; evidence from the highpressure subduction me´lange of New Caledonia. Contribution to Mineralogy and Petrology, 155, 181–198.

Ventruti, G., Mugnaioli, E., Capitani, G., Scordari, F., Pinto, D., and Lausi, A. (2015) A structural study of cyanotrichite from Dachang by concentional and automated electron diffraction. Physics and Chemistry of Minerals, 42, 651-661.

Vincent, R., and Midgley, P.A.(1994) Double conical beam-rocking system for measurement of integrated electron diffraction intensities. Ultramicroscopy, 53, 271–282.

Welch, M., and Marshhall, W.G. (2001) High-pressure behavior of clinochlore. American Mineralogist, 86, 1380-1386.

Tables

Run name	Bulk composition	P (GPa)	T (°C)	Runtime (h)	Phase
A8	A (Cr-MASH)	6.5	700	150	Py, Fo, 11.5 Å, Gu
B5	B (Cr-MASH)	6.0	650	168	Fo, Gu, Cen, HySo
B6	B (Cr-MASH)	6.5	700	150	Fo, Gu, Cen, HySo
JO1	JO (MASH)	6.5	700	218	Fo, 11.5 Å, HySo

Table 1. Details of the synthesis conditions of experiments involving 11.5 Å or HySo phases. Py: pyrope, Fo: forsterite, Gu: guyanaite, Cen: clinoenstatite.

583

	11.5 Å	HySo
Data Set		
Angular range (°)	-60 to +50	-51 to +60
N. of patterns	111	112
Angular step (°)	1	1
Precession angle (°)	1	2
Kinematical Refinement		
N. of reflections (obs/all)	432/1770	1387/2352
N. of independent reflections (obs/all)	200/709	572/813
N. of refined parameters:	35	41
R (obs/all) (%)	19.67/37.09	27.49/29.90
wR (obs/all) (%)	20.78/21.14	30.88/30.97
Goodness of fit (obs/all)	9.97/5.02	12.97/15.58
Dynamical Refinement		
N. of reflections (obs/all)		2463/5259
N. of refined parameters		151
g_{max}(Å^{-1})		2
Sg_{max} (matrix) (Å^{-1})		0.01
Sg_{max} (refine) (Å^{-1})		.1
R_{Sg}^{max}		0.4
Refined thickness (nm)		55.9(2)
R (obs/all) (%)		9.49/15.88
wR (obs/all) (%)		10.27/12.05
Goodness of fit (obs/all)		1.97/2.44

584

585 Table 2. Details of the structure refinement results for the 11.5 and the HySo phases. The reported
586 parameters for the dynamical refinements calculations are defined in Palatinus et al. (2015a-b).
587

Name	Chemical formula	Space group	Density (g/cm3)	Ref.
Clinochlore	$Mg_5(Mg_{0.1}Al_{1.2}Cr_{0.7})(Si_3O_{10})(OH)_8$	C-1	2.69	1
Hapy	$Mg_{2.1}Al_{0.9}(OH)_2Al_{0.9}Si_{1.1}O_6$	C 2/m	3.175	2
11.5 Å	$Mg_6Al(OH)_7(SiO_4)_2$	C 2/c	2.93	This work
Hyso	$Mg_3Al(OH)_3(Si_2O_7)$	C 2/m	3.13	This work
Mg-sursassite	$Mg_4(Mg_{0.42}Al_{0.58})_2(Al_4Si_6O_{21.16})(OH)_{6.84}$	$P2_1/m$	3.27	4

588

589 Table 3. Composition, symmetry and density of the main high pressure hydrous phases of the
590 MASH system. All phases have very low symmetry, either triclinic or monoclinic. References: 1-
591 Brown and Bailey 1963, 2 - Gemmi et al. 2011, 3 - Gottschalk et al. 2000.
592

593

594

595 **Figure captions**

596

Figure 1. fEDT screening on two crystal aggregates. In the two boxes the bright field images of the aggregates and the three dimensional reconstructions of the reciprocal space based on the fEDT data collection on the marked crystals are displayed (Py-pyrope, Fo-forsterite, Mg-magnesite, 11.5-11.5 Å phase, Gu-Guyanaite). All the investigated crystals have a size of 500nm or smaller and are in contact with other crystals requiring a remarkable goniometer for an automatic fEDT data collection.

Figure 2. Three dimensional reconstruction of the reciprocal space of a disordered crystal of 11.5 Å phase A) Projection along the disordered stacking direction. Traces of the sections displayed in C) and D) are indicated by arrows and thin lines. B) View orthogonal to the disordered stacking direction showing the characteristic streaking. C) Sections normal to [100] zone axis. The streaking is not so pronounced and the vertical rows not passing through the origin show a double periodicity of 23 Å. D) Sections normal to [110] zone axis. The streaking in the vertical rows is evident but it does affect all the rows in the same way. One in every three rows is almost streaking-free.

Figure 3. Three dimensional reconstruction of the reciprocal space of an ordered crystal of 11.5 Å phase. Projections along the three fundamental reciprocal directions, (001), (010) and (100) are displayed. For comparison a section normal to [110] zone axis corresponding to the same displayed in fig.1 D) is shown at bottom right. The strong streaking parallel to (001) has completely disappeared.

Figure 4. Structural model of the 11.5 Å phase. Color code: orange Mg; light blue Al; blue Si; red O; green OH. 1) [010] projection. 2) [100] projection 3) The double octahedral layer viewed along **c***. 4) One TOT layer viewed along **c***.

Figure 5. a) Stacking sequence of two unit cells along **c** of the 11.5 Å phase viewed along the [110] direction. In this projection the s+ and s- modules can be distinguished. b) High resolution image taken near the edge of on crystal of 11.5 Å phase in [110] orientation. c) the same image filtered by averaging out the contribution of the amorphous scattering. A simulated image is reported in the inset. The disordered stacking sequence of the different TOT modules is evident. d) Simulated

623 image (in the conditions matching the image contrast) superimposed on the crystal structure of an
624 ordered unit cell stacking. The strong white dots correspond to the OH group in between the TOT
625 modules, while the weakest white dots correspond to the empty spaces between the tetrahedra of the
626 TOT modules. Their parallel or staggered configuration corresponds to the s+ and s- module type,
627 respectively.
628 Figure 6. Rietveld analysis of the sample JO1 (circles: experimental data points; black line: Rietveld
629 fit; gray line: difference curve). In the inset a portion of the low angle powder pattern is plotted and
630 the diffraction peaks are labelled (11.5: 11.5 Å phase; Fo: forsterite; Hy: HySo).
631 Figure 7. Projections of the 3D reconstructed reciprocal space of the new hydrous sorosilicate
632 phase along the (100), (010) and (001) reciprocal directions and along the rotation axis (top right).
633 Figure 8. A) Crystal structure of HySo viewed along the ***c*** axis. Color code: orange Mg; light blue
634 Al; blue Si; red O; green OH. The gray atoms correspond to the partially occupied Mg sites in
635 special position. B) TOT layer view normal to (100) planes. The displayed area corresponds to 2 x 2
636 unit cells. C) Difference Fourier map calculated taking into account dynamical scattering
637 superimposed on the structural model viewed along ***c***. The black atoms are oxygens, the dark gray
638 atoms are octahedral cations and the light gray atoms are tetrahedral silicon sites. The two new
639 tetrahedral sites T2 and T3 are clearly visible in the map. D) TOT layer as displayed in B) but with
640 the new tetrahedral sites in yellow. The M4 and M5 octahedral sites partially occupied are both
641 displayed in gray.
642

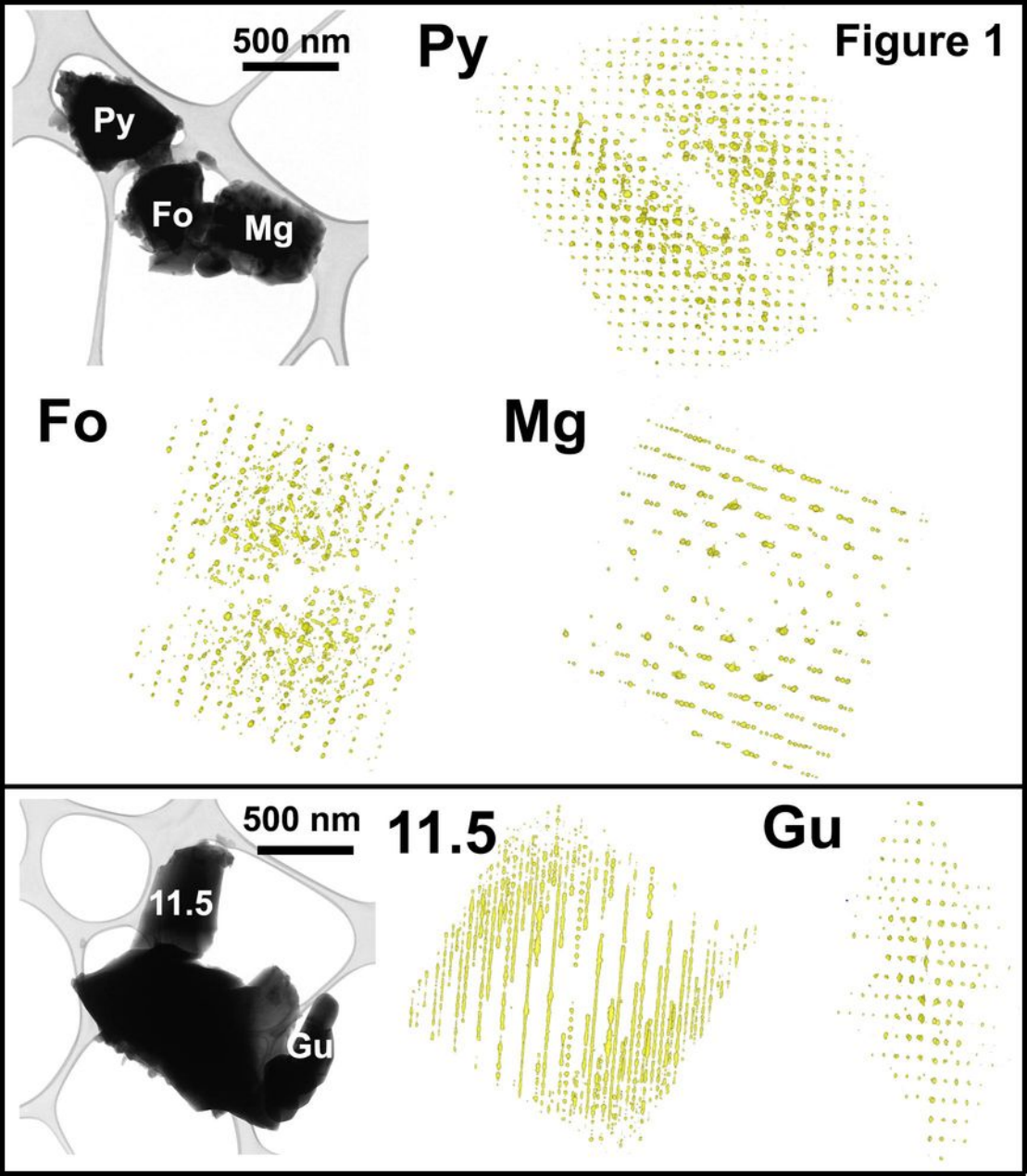
500 nm
Py
Fo
Mg
Py
Figure 1
Fo
Mg
500 nm
11.5
Gu
11.5
Gu

Figure 2

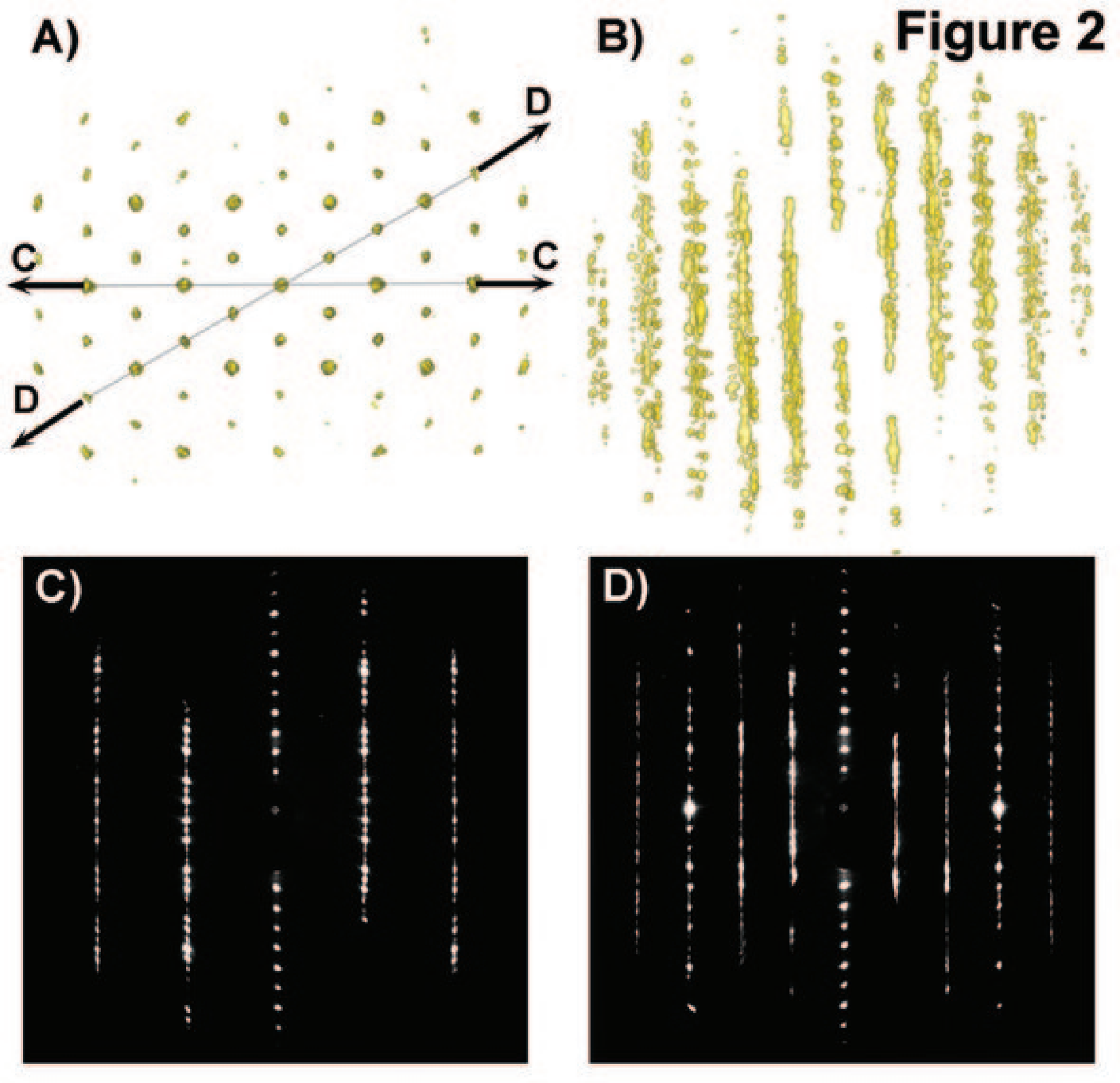

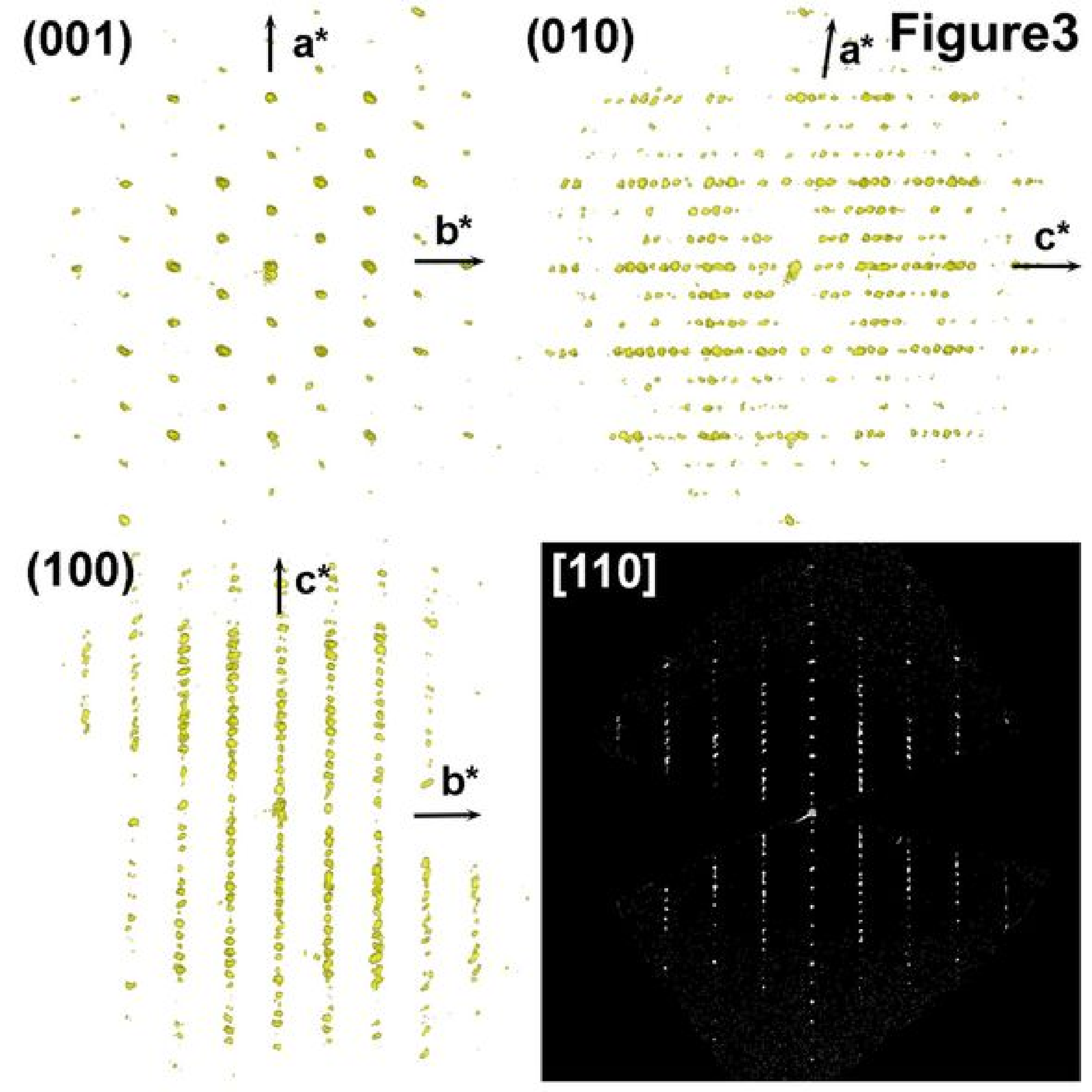

Figure3

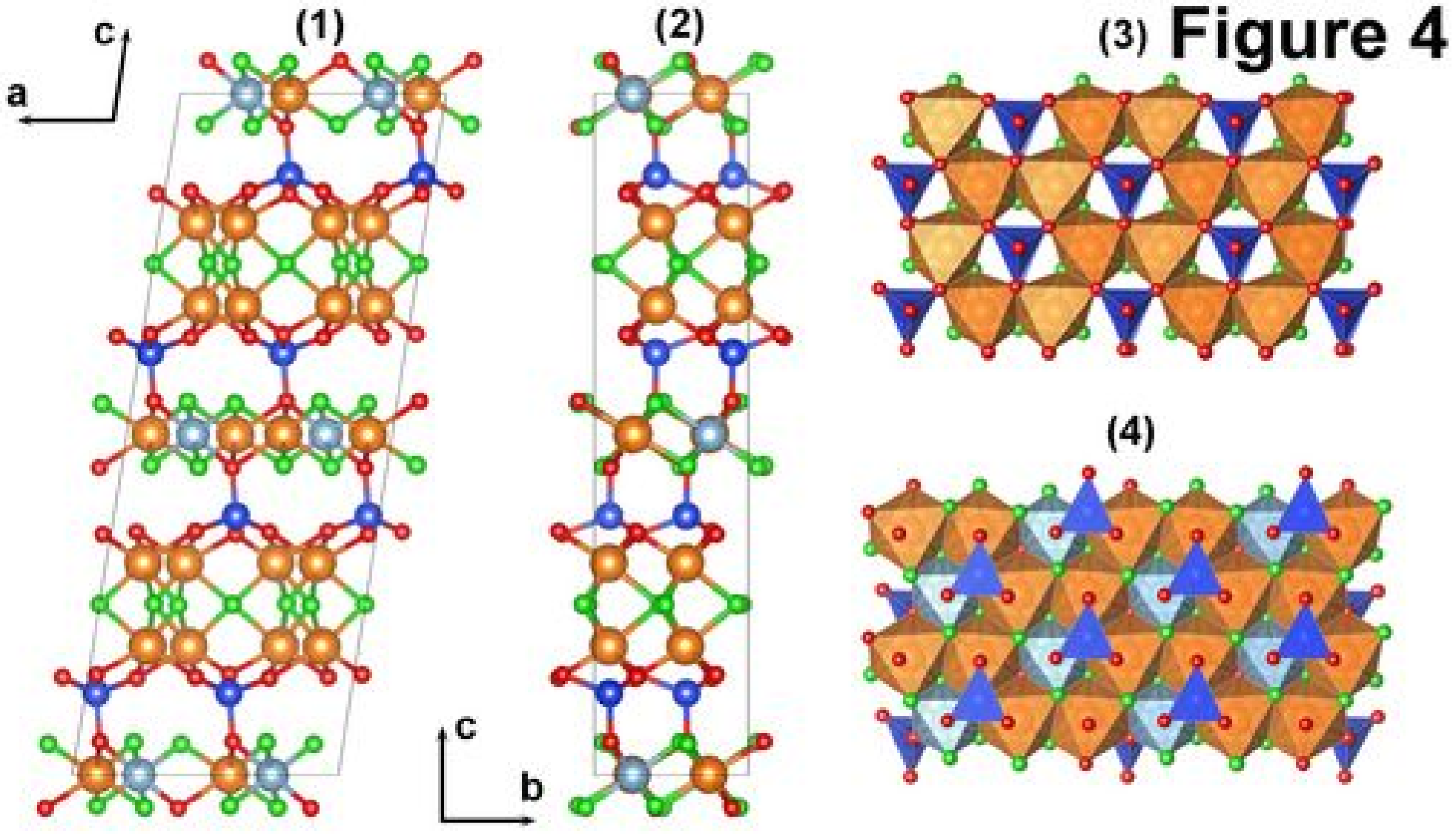

Figure 4

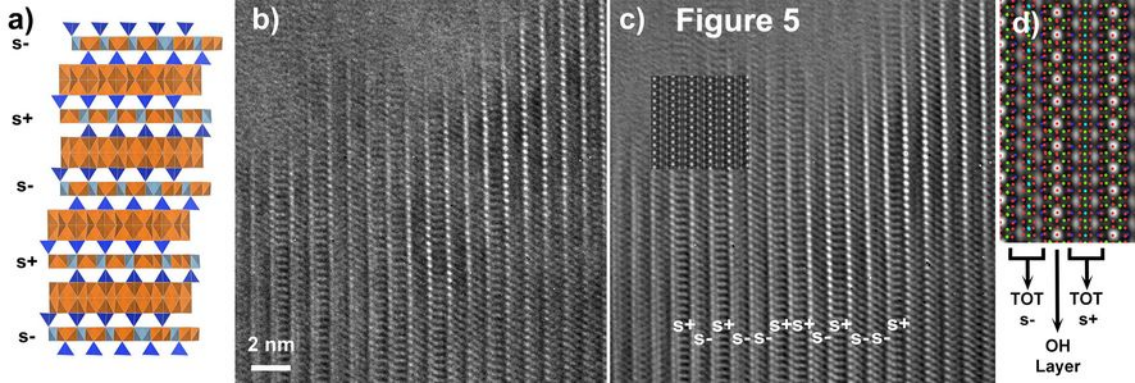
a)
s-
s+
s-
s+
s-
b)
2 nm
c)
Figure 5
s+ s- s+ s- s- s+ s+ s- s+ s- s- s+
d)
TOT
s-
TOT
s+
OH
Layer

JO1

Intensity (a.u.)

25000
20000
15000
10000
5000
0
-5000
-10000

0
5
10
15
20
25
30

2 theta (°)

6000
5000
4000
3000
2000
1000
0

2
3
4
5

11.5
Hy
Hy
11.5
Hy
Fo
Hy
11.5

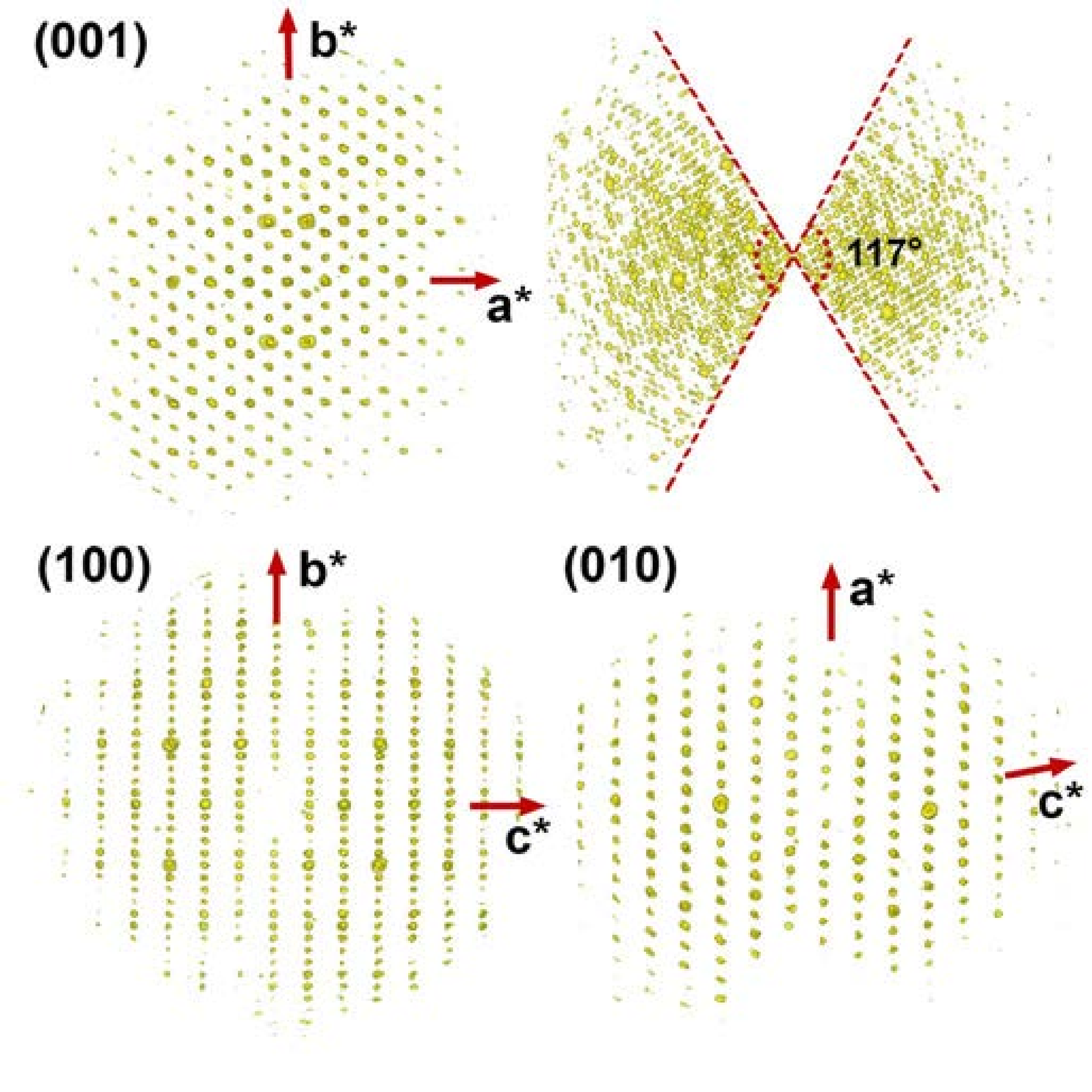
(001)
b*
a*
117°
(100)
b*
c*
(010)
a*
c*

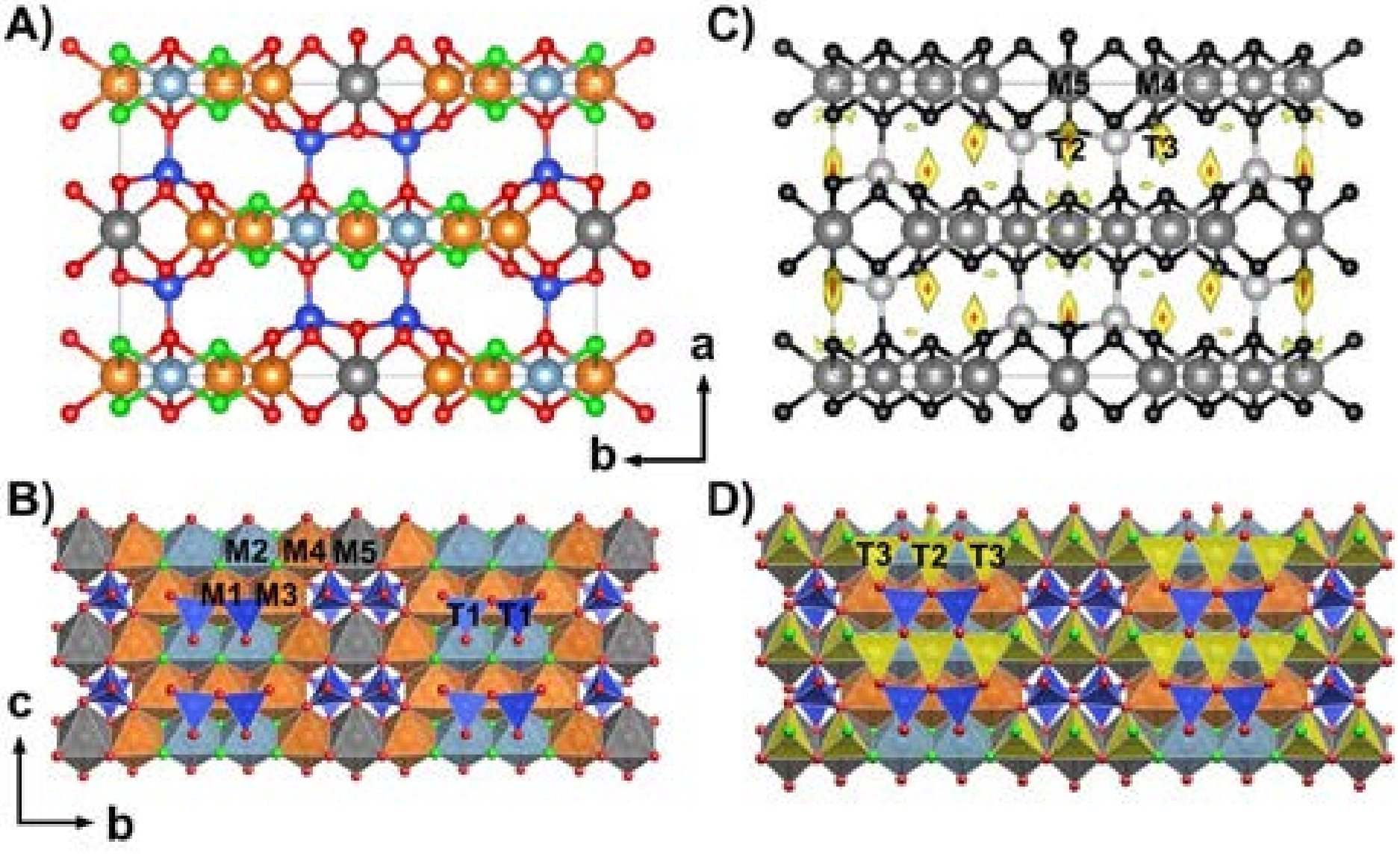
A)
a
b
C)
M5
M4
T2
T3
B)
M2 M4 M5
M1 M3
T1 T1
c
b
D)
T3 T2 T3